Journal of Pure and Applied Mathematics: Advances and Applications
Volume 12, Number 2, 2014, Pages 181-206

SLIP EFFECTS ON UNSTEADY MHD STAGNATION POINT FLOW OF A NANOFLUID OVER STRETCHING SHEET IN A POROUS MEDIUM WITH THERMAL RADIATION

F. M. HADY[1], MOHAMED R. EID[2] and MOSTAFA A. AHMED[3]

[1]Department of Mathematics
Faculty of Science
Assiut University
Assiut 71516
Egypt
e-mail: fekrymh@hotmail.com

[2]Department of Mathematics
Faculty of Science
New Valley Branch
Assiut University 72111
Egypt
e-mail: m_r_eid@yahoo.com

[3]Department of Mathematics
Faculty of Science
Sohag University
Sohag 82524
Egypt
e-mail: mostafa.abdallah@yahoo.com

2010 Mathematics Subject Classification: 76D10, 76S05, 76W05, 80A10.
Keywords and phrases: magnetic field, nanofluid, porous media, slip velocity, thermal radiation.
Received July 11, 2014

Abstract

In this article, the unsteady stagnation point flow and heat transfer of a nanofluid over a stretching sheet with the effects of magnetic field and porous media is investigated numerically. The effects of thermal radiation are also considered. In contrast to the conventional no-slip condition at the surface, Navier's slip condition has been applied. The behaviour of the nanofluid was investigated for three different nanoparticles in the water-base fluid, namely, copper, alumina, and titanium. The similarity solution is used to reduce the governing system of partial differential equations to a set of nonlinear ordinary differential equations, which are then solved numerically by using the fourth-order Runge-Kutta method along with shooting technique. The results corresponding to the dimensionless velocity and temperature profiles, also the skin friction and the reduced Nusselt number are displayed graphically for various pertinent parameters.

1. Introduction

At the macroscopic level, it is well accepted that the boundary condition for a viscous fluid at a solid wall is one of "no-slip", i.e., the fluid velocity matches the velocity of the solid boundary. While the no-slip boundary condition has been proven experimentally to be accurate for a number of macroscopic flows, it remains on assumption that is not based on physical principles. In fact, nearly two hundred years ago, Navier proposed a general boundary condition that incorporates the possibility of fluid slip at a solid boundary. Navier's proposed condition assumes that the velocity, ν_x, at a solid surface is proportional to the shear stress at the surface [1, 2].

$$\nu_x = \lambda(d\nu_x / dy),$$

where λ is the slip strength or slip coefficient. If $\lambda = 0$, then the general assumed no-slip boundary condition is obtained. If λ is finite, fluid slip occurs at the wall but its effect depends upon the length scale of the flow. The above relation states that the velocity of the fluid at the plates is linearly proportional to the shear stress at the plate. Also, one could impose nonlinear slip boundary conditions (e.g., [3]).

The fluid slippage phenomenon at the solid boundaries appear in many applications such as in microchannels or nanochannels and in applications, where a thin film of light oil is attached to the moving plates or when the surface is coated with special coatings such as thick monolayer of hydrophobic octadecyltrichlorosilane [4]. Also, wall slip can occur in the working fluid contains concentrated suspensions [5]. However, the literature lacks studies that take into account the possibility of fluid slippage at the wall under vibrating conditions. Recently, several researchers have suggested that the no-slip boundary condition may not be suitable for hydrophilic flows over hydrophobic boundaries at both the micro and nanoscale (for detailed study, the reader is referred to see [6-8]). The effect of the fluid slippage at the wall for coutte flow are considered by Marques et al. [9] under steady state conditions and only for gases. The closed form solution for steady periodic and transient velocity field under slip condition have been studied by Khaled and Vafai [10]. The effect of slip condition on MHD steady flow in a channel with permeable boundaries has been discussed by Makinde and Osalusi [11].

Stagnation flow occurs whenever a flow impinges onto a solid object and is of considerable technical relevance, for example, in turbo-machinery, flows over the submarines and oil ships or the leading edge of an aerofoil. In the stagnation region, pressure is at its maximum value and the highest rates of heat transfer and mass deposition occur. Wang [12] studied the concept of the flow of liquid film on an unsteady stretching surface. Bachok et al. [13] presented a similarity solution for the unsteady flow and heat transfer of a nanofluid over a permeable stretching/shrinking sheet and found that dual solutions exist for both stretching and shrinking cases. Suali et al. [14] studied the effects of suction and injection into the boundary layer on the unsteady stagnation point flow over a stretching/shrinking sheet. Fang et al. [15] analyzed the effect of unsteadiness on the viscous flow over an expanding stretching cylinder. Malvandi et al. [16] deals with the effects of slip velocity and

stretching parameter on the unsteady stagnation point flow of a nanofluid over a stretching sheet, where velocity of the sheet and free stream vary continuously with time. The boundary layer flow due to a stretching surface is important in extrusion processes, such as metal sheet extrusion, polymer extrusion, and other industrial processes such as hot rolling, drawing, crystal growth, paper production, and food production. In elastic materials under constant strain, stretching velocity is linearly increasing with the increase of distance from the leading edge.

MHD plays an important role in power generation, space propulsions, cure of diseases, control of thermonuclear reactor, and boundary layer control in field of aerodynamics. Magnetohydrodynamics (MHD) is the study of the flow of electrically conducting fluids in a magnetic field. Many experimental and theoretical studies on conventional electrically conducting fluids indicate that magnetic field markedly changes their transport and heat transfer characteristics. The unsteady boundary layer flow over a stretching sheet has been studied by Devi et al. [17], Elbashbeshy and Bazid [18], Tsai et al. [19], and Ishak [20].

Nanofluids with or without the presence of magnetic field have many applications in the industries since materials of nanometer size have unique chemical and physical properties. With regard to the sundry applications of nanofluids, the cooling applications of nanofluids include silicon mirror cooling, electronics cooling, vehicle cooling, transformer cooling, etc. This study is more important in industries such as hot rolling, melt spinning, extrusion, glass fiber production, wire drawing, manufacture of plastic and rubber sheets, polymer sheet and filaments, etc. The research on nanofluids is gaining a lot of attention in recent years. Pop et al. [21] have studied the radiation effect on the flow near the stagnation point of a stretching sheet. Abu-Nada [22] have state the application of nanofluids for heat transfer enhancement of separated flows encountered in a backward facing step. Kumar [23] has discussed about radiative heat transfer with hydro magnetic flow and viscous dissipation over a stretching surface in the presence of variable heat flux.

The thermal radiation effects becomes intensified at high absolute temperature levels due to basic difference between radiation and the convection and conduction energy-exchange mechanisms. In the context of space technology, some devices for space applications are designed to operate at high temperature levels in order to achieve high thermal efficiency. Hence, the effects of radiation are of vital importance when calculating thermal effects in the processes involving high temperatures. Thus, Akbar et al. [24] studied radiation effects on MHD stagnation point flow of nanofluid towards a stretching surface with convective boundary condition. Nadeem et al. [25] examined heat transfer analysis of water-based nanofluid over an exponentially stretching sheet. In all these works, the linear approximation to the thermal radiation model is used based on the assumption that the temperature differences within the flow are so small that T^4 can be expressed as a linear function of T_∞, which is obtained by expending T^4 in Taylor series about T_∞ and neglecting the higher order terms.

The objective of this paper is to present a detailed study on the development of the unsteady 2D boundary layer flow and heat transfer of a viscous nanofluid in the region of the stagnation point on a stretching sheet in a porous medium in the presence of thermal radiation. A transverse magnetic field is applied and the fluid is assumed to be incompressible. Using a similarity transformation, the Navier-Stokes equations are reduced to a set of nonlinear ordinary differential equations. The resulting nonlinear system is solved numerically for three different types of nanofluids, namely, copper (Cu), alumina (Al_2O_3), and titanium dioxide (TiO_2), using the fourth-order Runge-Kutta method with shooting technique. The results obtained are then compared with those of Bachok et al. [13] and Malvandi et al. [16]. We restrict our study to a common Prandtl number for nanofluids, taking Pr = 6.2. For other values of Pr, we expect to have qualitatively similar results.

2. Problem Formulations

Consider an incompressible unsteady viscous flow of nanofluids being confined to $y > 0$ toward a stretching sheet coinciding with the plane at $y = 0$ with a fixed stagnation point at $x = 0$ as shown in Figure 1. We have assumed that the free stream and sheet's velocity vary with time from a fixed stagnation point in the form of $U_e(x, t) = ax(1 - ct)^{-1}$ and $U_w(x, t) = bx(1 - ct)^{-1}$, respectively, where a, b, and c are positive constants. Current assumptions are necessary in order to provide a similarity solution. It is also assumed that the temperature at the surface has a constant value of T_w, while the ambient temperature beyond the boundary layer has a constant value of T_∞. The basic unsteady conservation equations of mass, momentum, and thermal energy can be expressed as, see Bachok et al. [26]

$$\frac{\partial u}{\partial x} + \frac{\partial \nu}{\partial y} = 0, \tag{1}$$

$$\frac{\partial u}{\partial t} + u\frac{\partial u}{\partial x} + \nu\frac{\partial u}{\partial y} = \frac{\partial u_e}{\partial t} + u_e\frac{du_e}{dx} + \frac{\mu_{nf}}{\rho_{nf}}\left(\frac{\partial^2 u}{\partial x^2} + \frac{\partial^2 u}{\partial y^2}\right) + \frac{\mu_{nf}}{\rho_{nf}K_1}(u_e - u) + \frac{\sigma B^2}{\rho_{nf}}(u_e - u), \tag{2}$$

$$\frac{\partial T}{\partial t} + u\frac{\partial T}{\partial x} + \nu\frac{\partial T}{\partial y} = \alpha_{nf}\left(\frac{\partial^2 T}{\partial x^2} + \frac{\partial^2 T}{\partial y^2}\right) - \frac{1}{(\rho C_p)_{nf}}\frac{\partial q_r}{\partial y}. \tag{3}$$

The boundary conditions suggested by the physics of the problem are given by

$$u = U_w(x, t) + U_{slip}(x, t), \quad \nu = 0; \quad T = T_w \quad \text{at } y = 0;$$

$$u \to U_e(x, t) = ax(1 - ct)^{-1}; \quad T \to T_\infty \quad \text{as } y \to \infty. \tag{4}$$

Here u and ν are the velocity components along the x and y directions, respectively, $U_{slip}(x, t) = N_1 \upsilon \frac{\partial u}{\partial y}$, where $N_1 = N\sqrt{t}$ is the slip velocity factor and t is the time. T is the temperature, B is the uniform magnetic field strength, σ is the electrical conductivity of fluid, K_1 is the uniform permeability of the porous medium, q_r is the radiative heat flux, μ_{nf} is the viscosity of nanofluid, ρ_{nf} is the density of nanofluid, α_{nf} is the thermal diffusivity, and $(\rho C_p)_{nf}$ is the heat capacitance of the nanofluid which for spherical nanoparticles are (see Oztop and Abu-Nada [27])

$$\rho_{nf} = (1-\phi)\rho_f + \phi\rho_s; \quad \mu_{nf} = \frac{\mu_f}{(1-\phi)^{2.5}}; \quad \alpha_{nf} = \frac{k_{nf}}{(\rho C_p)_{nf}};$$

$$(\rho C_p)_{nf} = (1-\phi)(\rho C_p)_f + \phi(\rho C_p)_s;$$

$$\frac{k_{nf}}{k_f} = \frac{(k_s + 2k_f) - 2\phi(k_f - k_s)}{(k_s + 2k_f) + 2\phi(k_f - k_s)}, \tag{5}$$

where ϕ is the solid volume fraction of the nanofluid, μ_f is the viscosity of the basic fluid, ρ_f and ρ_s are the densities of the pure fluid and nanoparticle, respectively, $(\rho C_p)_f$ and $(\rho C_p)_s$ are the specific heat parameters of the base fluid and nanoparticle, respectively, k_f and k_s are the thermal conductivities of the base fluid and nanoparticle, respectively.

To obtain similarity transformation, it is assumed that the magnetic field B and the permeability of the porous medium K_1 are of the form

$$K_1 = K(1 - ct), \qquad B = \frac{B_o}{\sqrt{1 - ct}},$$

where K is permeability of the porous medium and B_o is the constant magnetic field.

We are interested in similarity solution of the above boundary value problem; therefore, we introduce the following dimensionless variables:

$$\psi = \left(\frac{\upsilon_f a}{(1-ct)}\right)^{1/2} xf(\eta), \quad \eta = y\left(\frac{a}{\upsilon_f(1-ct)}\right)^{1/2}, \quad \theta(\eta) = \frac{T-T_\infty}{T_w - T_\infty}. \quad (6)$$

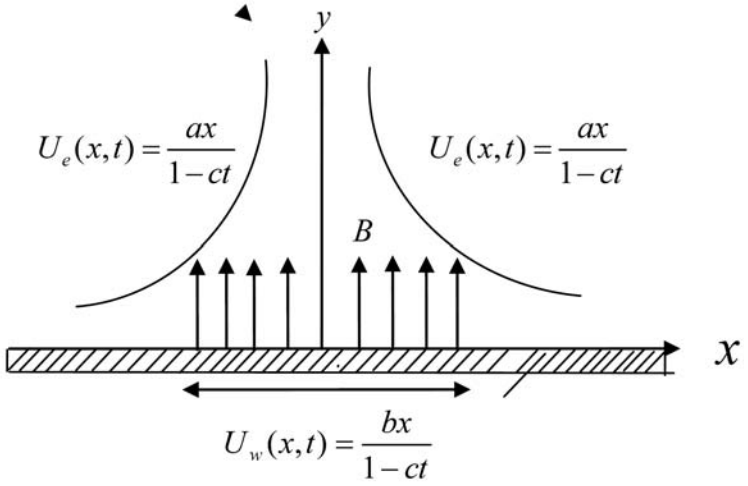

Figure 1. Physical model and coordinate system.

Using the Rosseland approximation for thermal radiation and applying to optically thick media, the radiative heat flux is given by (Raptis [28], Brewster [29], and Sparrow and Cess [30])

$$q_r = -\frac{4\sigma^*}{3k^*}\frac{\partial T^4}{\partial y} = -\frac{16\sigma^*}{3k^*}T^3\frac{\partial T}{\partial y}, \quad (7)$$

where σ^* and k^* are the Stefan-Boltzmann constant and the mean absorption coefficient, respectively. Now Equation (3) can be expressed as

$$\frac{\partial T}{\partial t} + u\frac{\partial T}{\partial x} + v\frac{\partial T}{\partial y} = \alpha_{nf}\left(\frac{\partial^2 T}{\partial x^2} + \frac{\partial^2 T}{\partial y^2}\right) + \frac{1}{(\rho C_p)_{nf}}\frac{16T_\infty^3\sigma^*}{3k^*}\frac{\partial^2 T}{\partial y^2}. \quad (8)$$

By using the non-dimensional transformations (6), we get the following system of non-dimensional equations:

$$f''' + \left(\kappa + M(1-\phi)^{2.5}\right)(1-f') + (1-\phi)^{2.5}\left(1-\phi+\phi\frac{\rho_s}{\rho_f}\right)$$

$$\times\left(f''\left(f-\frac{\eta A}{2}\right) - f'(A+f') + A + 1\right) = 0, \tag{9}$$

$$\left(\frac{k_{nf}}{k_f} + \frac{4R_d}{3}\right)\theta'' + \Pr\left(1-\phi+\phi\frac{(\rho C_p)_s}{(\rho C_p)_f}\right)\left(f - \frac{A}{2}\eta\right)\theta' = 0. \tag{10}$$

With the boundary conditions:

$$f' = \varepsilon + \lambda f'', \quad f = 0; \quad \theta = 1 \quad \text{at } \eta = 0;$$

$$f' \to 1; \quad \theta \to 0 \quad \text{as } \eta \to \infty, \tag{11}$$

where

$$\Pr = \frac{\upsilon_f}{\alpha}, \quad \varepsilon = \frac{b}{a}, \quad A = \frac{c}{a}, \quad \lambda = N\left(\frac{\upsilon_f at}{(1-ct)}\right)^{1/2},$$

$$\kappa = \frac{\nu_f}{aK}, \quad M = \frac{\sigma B_o^2}{a\rho_f}, \quad R_d = \frac{4T_\infty^3\sigma^*}{k_f k^*}. \tag{12}$$

Here Pr, ε, A, λ, κ, M, and R_d denote a Prandtl number for the base fluid, the stretching parameter, the unsteadiness parameter, the slip parameter, the porous media parameter, the magnetic field parameter, and the radiation parameter.

The physical quantities of the local skin friction coefficient Cf_x and the reduced Nusselt number Nu_x are calculated, respectively, by the following:

$$Cf_x = \frac{\tau_w}{\rho_f U_w^2}, \qquad Nu_x = \frac{xq_w}{k_f(T_w - T_\infty)}, \tag{13}$$

where τ_w is the surface shear stress and q_w is the surface heat flux which are given by

$$\tau_w = \mu_{nf}\left(\frac{\partial u}{\partial y}\right)_{y=0}, \qquad q_w = -k_{nf}\left(\frac{\partial T}{\partial y}\right)_{y=0}. \tag{14}$$

Using Equations (13) and (14), we obtain

$$Cfr = \mathrm{Re}_x^{1/2}\, Cf_x = \frac{1}{(1-\phi)^{2.5}} f''(0), \qquad Nur = \mathrm{Re}_x^{-1/2}\, Nu_x = -\frac{k_{nf}}{k_f}\theta'(0),$$

where $\mathrm{Re}_x = xU_w / \upsilon_f$ is the local Reynolds number.

3. Numerical Method

An efficient fourth-order Runge-Kutta method along with shooting technique has been employed to study the flow model for the above coupled non-linear ordinary differential equations (Equations (9) and (10)) for different values of governing parameters viz. Prandtl number Pr, the slip parameter λ, the porous media parameter κ, the magnetic field parameter M, and the radiation parameter R_d. The non-linear differential equations are first decomposed into a system of first-order differential equation. The coupled ordinary differential equations (9) and (10) are third-order in f and second-order in θ, which have been reduced to a system of five simultaneous equations for five unknowns. In order to numerically solve this system of equations using Runge-Kutta method, the solution requires five initial conditions but two initial conditions in f one initial condition in θ are known. However, the values of f' and θ are known at $\eta \to \infty$. These end conditions are utilized to produce unknown initial conditions at $\eta = 0$ by using shooting technique. The most important step of this scheme is to choose the appropriate finite value of η_∞. Thus to estimate the value of η_∞, we start with some initial guess value and solve the boundary value problem consisting of Equations (9) and (10) to obtain $f''(0)$ and $-\theta'(0)$. The solution process is repeated with another larger value of η_∞ until two successive values of

$f''(0)$ and $-\theta'(0)$ differ only after desired significant digit. The last value η_∞ is taken as the finite value of the limit η_∞ for the particular set of physical parameters for determining velocity and temperature, respectively, are $f'(\eta)$ and $\theta(\eta)$ in the boundary layer. After getting all the initial conditions, we solve this system of simultaneous equations by using fourth-order Runge-Kutta integration scheme. The value of η_∞ is selected to vary from 5 to 20 depending on the physical parameters governing the flow so that no numerical oscillation would occur. Thus, the coupled boundary value problem of third-order in f and second-order in θ has been reduced to a system of five simultaneous equations of first-order for five unknowns as follows:

The Equations (9) and (10) can be expressed as:

$$f''' = -\left(\kappa + M(1-\phi)^{2.5}\right)(1-f') - (1-\phi)^{2.5}\left(1-\phi+\phi\frac{\rho_s}{\rho_f}\right) \times \left(f''\left(f-\frac{\eta A}{2}\right) - f'(A+f') + A + 1\right),$$

$$\theta'' = -\Pr\frac{\left(1-\phi+\phi\frac{(\rho C_p)_s}{(\rho C_p)_f}\right)\left(f-\frac{A}{2}\eta\right)\theta'}{\left(\frac{k_{nf}}{k_f}+\frac{4R_d}{3}\right)}.$$

Now we can define new variables by the equations

$$f_1 = f, \quad f_2 = f', \quad f_3 = f'', \quad f_4 = \theta, \quad f_5 = \theta'.$$

The coupled higher order non-linear differential equations and the boundary conditions may be transformed to five equivalent first-order differential equations and boundary conditions, respectively, as given below:

$$f_1' = f_2,$$

$$f_2' = f_3,$$

$$f_3' = -\left(\kappa + M(1-\phi)^{2.5}\right)(1-f') - (1-\phi)^{2.5}\left(1-\phi+\phi\frac{\rho_s}{\rho_f}\right)$$

$$\times\left(f''\left(f-\frac{\eta A}{2}\right) - f'(A+f') + A + 1\right),$$

$$f_4' = f_5,$$

$$f_5' = -\Pr\frac{\left(1-\phi+\phi\dfrac{(\rho C_p)_s}{(\rho C_p)_f}\right)\left(f-\dfrac{A}{2}\eta\right)\theta'}{\left(\dfrac{k_{nf}}{k_f}+\dfrac{4R_d}{3}\right)}.$$

A prime denote the differentiation with respect to η and the boundary conditions are

$$f_2(0) = \varepsilon + \lambda f_3(0), \quad f_1(0) = 0; \quad f_4(0) = 1;$$

$$f_2(\infty) \to 1; \quad f_4(\infty) \to 0.$$

In this study, the boundary value problem is first converted into an initial value problem (IVP). Then, the IVP is solved by appropriately guessing the missing initial value using the shooting method for several sets of parameters. The step size $h = 0.1$ is used for the computational purpose. The error tolerance of 10^{-7} is also being used. The results obtained are presented through tables and graphs, and the main features of the problems are discussed and analyzed.

4. Results and Discussion

The resulting differential systems (9) and (10) subjected to the boundary conditions (11) are solved numerically through fourth-order Runge-Kutta method along with shooting technique. The values of the governing parameters are chosen arbitrary. However, the numerical results are presented for some representative values of these governing parameters. In order to see the physical insight, the numerical values of

velocity $f'(\eta)$ and temperature $\theta(\eta)$ with the boundary layer have been computed for different parameters as the stretching parameter ε, the unsteadiness parameter A, the slip parameter λ, the porous media parameter κ, the magnetic field parameter M, and the radiation parameter R_d.

In order to verify the accuracy of the numerical results, the validity of the numerical code developed has been checked by direct comparisons with the numerical results reported earlier by Bachok et al. [13] and Malvandi et al. [16] for various values of reduced Nusselt number and skin friction coefficient for three different nanofluids, namely, copper (Cu), alumina (Al_2O_3), and titanium dioxide (TiO_2). Each nanofluid was suspended in water as the base fluid for which $Pr = 6.2$ for different values of ϕ as shown in Table 2. Thermophysical properties of the base fluid and the nanoparticles are shown in Table 1. The quantitative comparisons found to be in excellent agreement and thus give confidence that the numerical results obtained are accurate. The physical representation of the present study is shown in Figures 2-14.

Table 1. Thermo-physical properties of fluid and nanoparticles (Oztop and Abu-Nada [27])

Physical properties	Fluid phase (water)	Cu	Al_2O_3	TiO_2
C_p(J/kgK)	4179	385	765	686.2
ρ(kg/m^3)	997.1	8933	3970	4250
k(W/mK)	0.613	401	40	8.9538
$\beta \times 10^5$(K^{-1})	21	1.67	0.85	0.9

Table 2. Comparison of the values of $f''(0)$ and $-\theta'(0)$ when $\varepsilon = \lambda = \kappa = M = R_d = 0$

A	Material	ϕ	$f''(0)$			$-\theta'(0)$		
			Bachok et al. [13]	Malvandi et al. [16]	Present results	Bachok et al. [13]	Malvandi et al. [16]	Present results
1	Cu	0.1	1.7604	1.76039	1.76039	0.4681	0.46870	0.46813
		0.2	–	1.82528	1.82526	–	0.46779	0.46587
	Al_2O_3	0.1	1.4967	1.49669	1.49668	0.4032	0.40320	0.40324
		0.2	–	1.43248	1.43247	–	0.38477	0.38400
	TiO_2	0.1	1.5128	1.51280	1.51280	0.4076	0.40757	0.40756
		0.2	–	1.45746	1.45745	–	0.39199	0.39128
– 1	TiO_2	0.1	0.932	0.93199	0.93199	1.491	1.50207	1.49102
		0.2	–	0.89790	0.89790	–	1.35558	1.32640

Figures 2 and 3 display the dimensionless velocity distribution $f'(\eta)$ and the dimensionless temperature distribution $\theta(\eta)$ for different values of nanoparticle volume fraction ϕ for Cu-water nanofluid with $\mathrm{Pr} = 6.2$, $\lambda = 0.5$, $\varepsilon = 0.5$, $A = 1.0$, and $R_d = 0.5$. From these figures, it is noticed that both of $f'(\eta)$ and $\theta(\eta)$ increases for the increasing values of ϕ. In fact, as ϕ increases, there is an increase in the velocity field, i.e., the flow has boundary layer structure. It is important to note that the momentum boundary layer thickness in nonporous medium ($\kappa = 0$) and in the absence of magnetic field ($M = 0$) is lower to it in a porous medium with the presence of magnetic field ($\kappa = M = 1$) as shown in Figure 2, whereas reverse trend is observed for $\theta(\eta)$ as shown in Figure 3. Figure 4 illustrates typical profiles for velocity for different values of the porous media parameter κ and the magnetic field parameter M for Cu-water. As expected, we observed from this figure that the velocity profile $f'(\eta)$ is an increasing function of κ and M. Figure 5 shows the temperature profile for Cu-water nanofluids. It can be observed for this figure that temperature profile for Cu-water increases with increasing the radiation parameter R_d, while it decreases as the stretching parameter ε increases. Figure 6 shows that the influence of both the slip parameter λ and the unsteadiness parameter A for Cu-water working fluid on the dimensionless velocity distribution $f'(\eta)$. As both parameters increase, the velocity $f'(\eta)$ increases. For Cu-water working fluid, the temperature function $\theta(\eta)$ decreases as the slip parameter λ increases, but it increases as the unsteadiness parameter A increases as shown in Figure 7. The effects of the porous media parameter κ and the slip parameter λ on the skin-friction coefficient and Nusselt number for the three types of nanofluids (Cu-water), (Al_2O_3-water), and (TiO_2-water) are provided in Figures 8 and 9, respectively. It is observed from Figure 8 that the $f''(0)$ increases with increasing the value of κ, while $f''(0)$ decreases as

the slip parameter λ increases. It is seen that the Nusselt number $-\theta'(0)$ increases with increasing the value of both of κ and λ as shown in Figure 9. The same behaviour is observed for different values of M (Figure 11) for different nanoparticles. The $f''(0)$ increases with increasing the value of M as shown in Figure 10 for different nanoparticles. In Figure 12, the temperature gradient at the sheet (the Nusselt number) $-\theta'(0)$ which is proportional to the rate of heat transfer from the sheet is plotted for different values of the radiation parameter R_d for different nanoparticles. It is observed that $-\theta'(0)$ decreases with an increase in R_d.

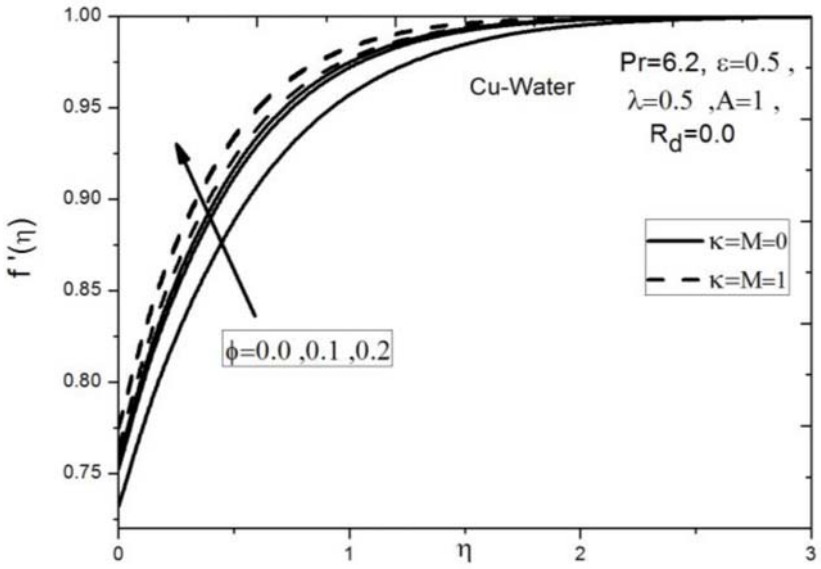

Figure 2. Effects of nanoparticle volume fraction ϕ for Cu-water working fluid on velocity profiles.

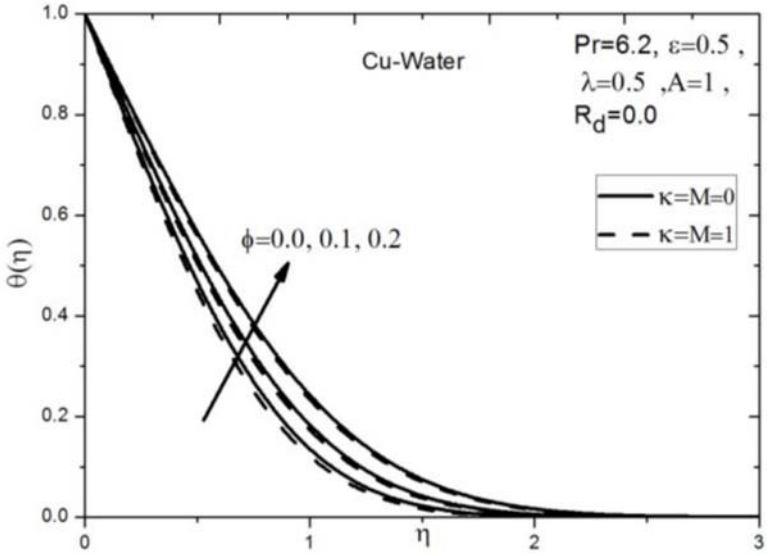

Figure 3. Effects of nanoparticle volume fraction ϕ for Cu-water working fluid on temperature function.

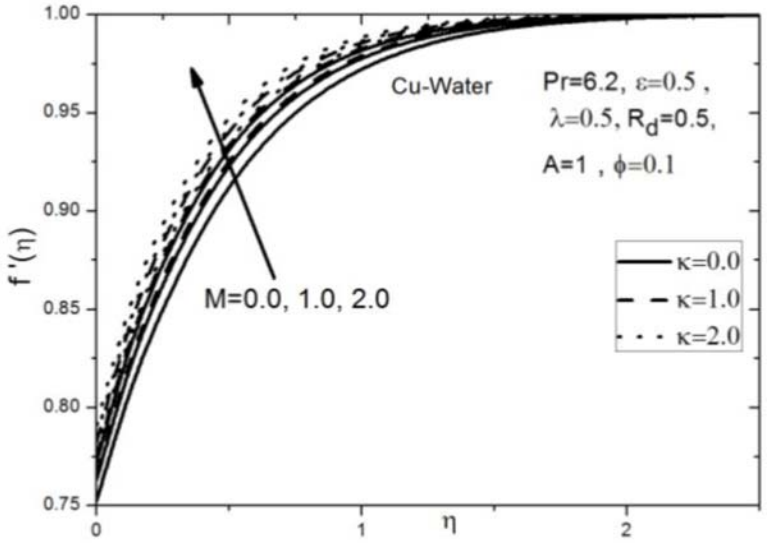

Figure 4. Effects of the porous media parameter κ and the magnetic field parameter M for Cu-water working fluid on velocity profiles.

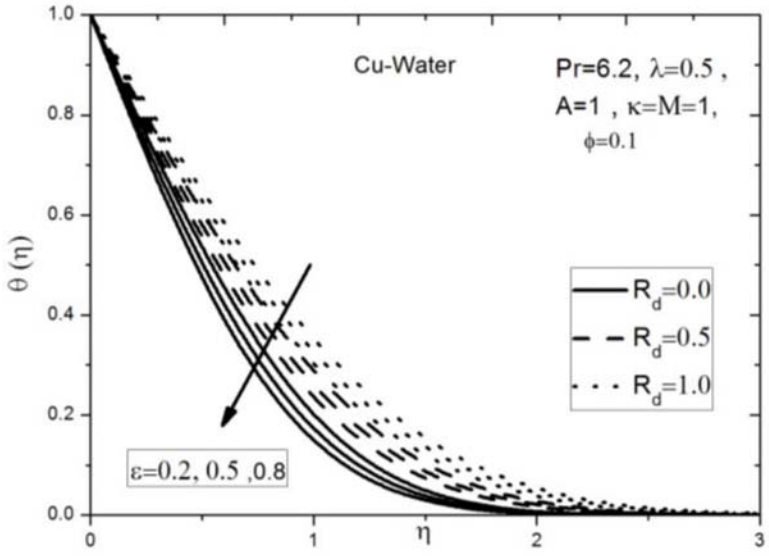

Figure 5. Effects of the stretching parameter ε and R_d for Cu-water working fluid on temperature function.

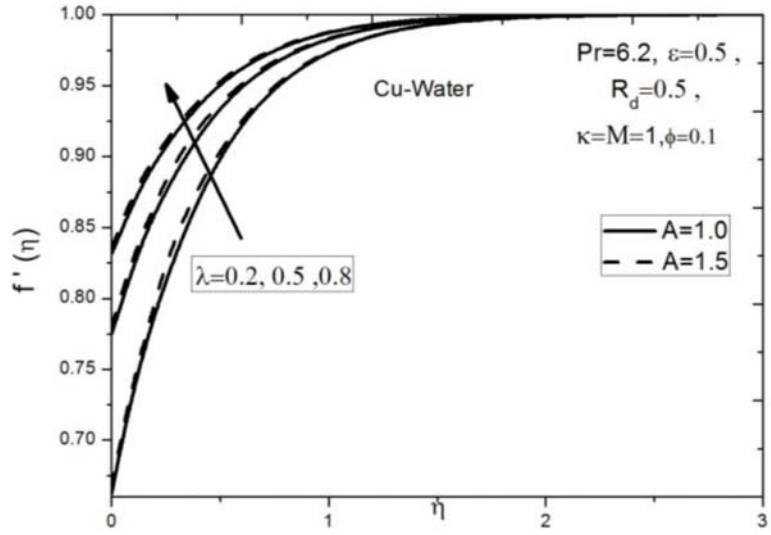

Figure 6. Effects of the slip parameter λ and A for Cu-water working fluid on velocity profiles.

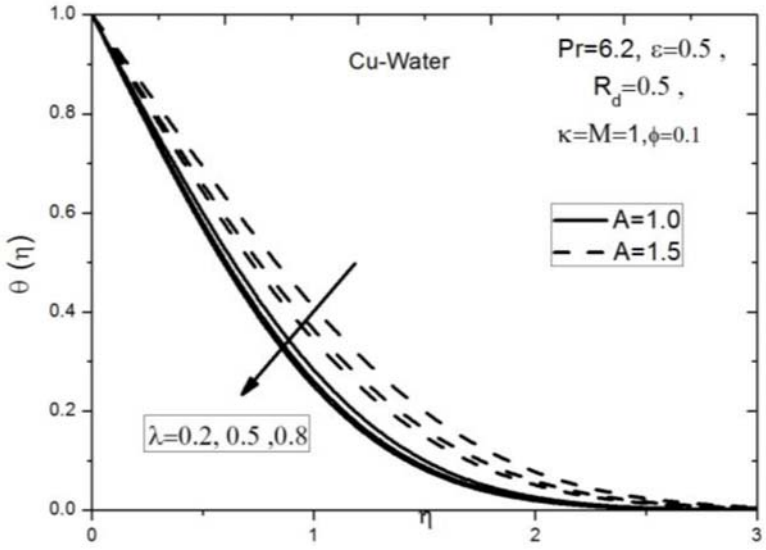

Figure 7. Effects of the slip parameter λ and A for Cu-water working fluid on temperature function.

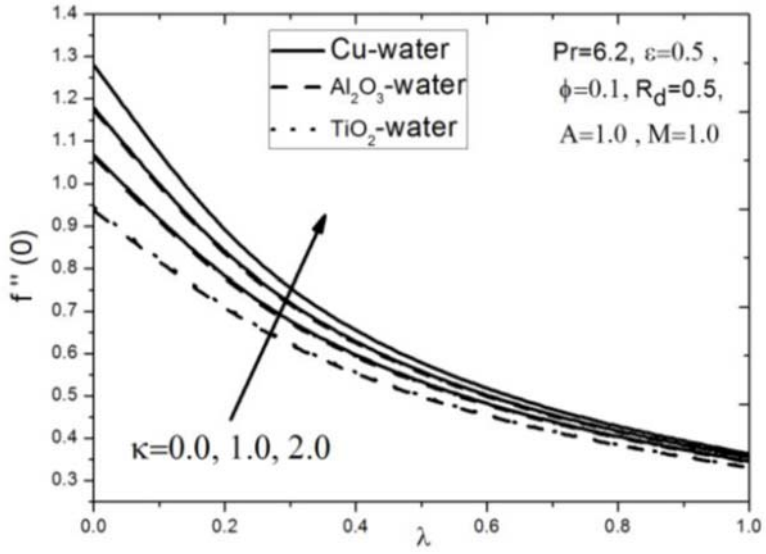

Figure 8. Effects of porous media parameter κ and λ on the skin friction coefficient.

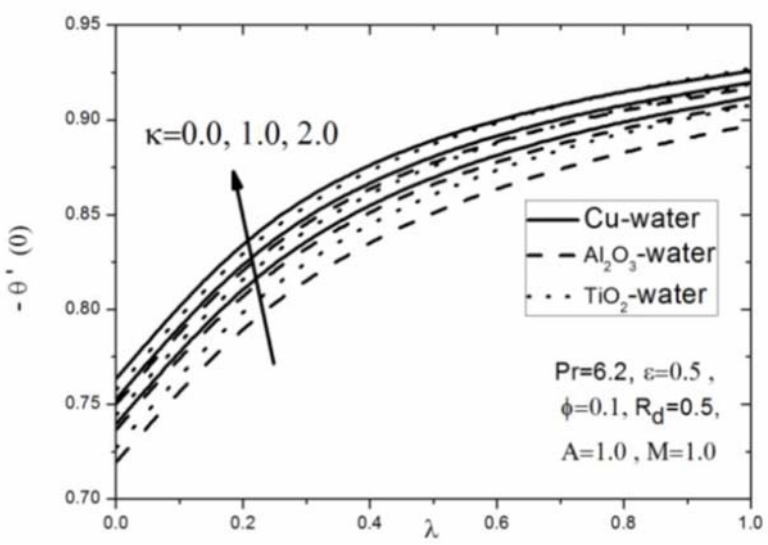

Figure 9. Effects of the porous media parameter κ and λ on the reduced Nusselt number.

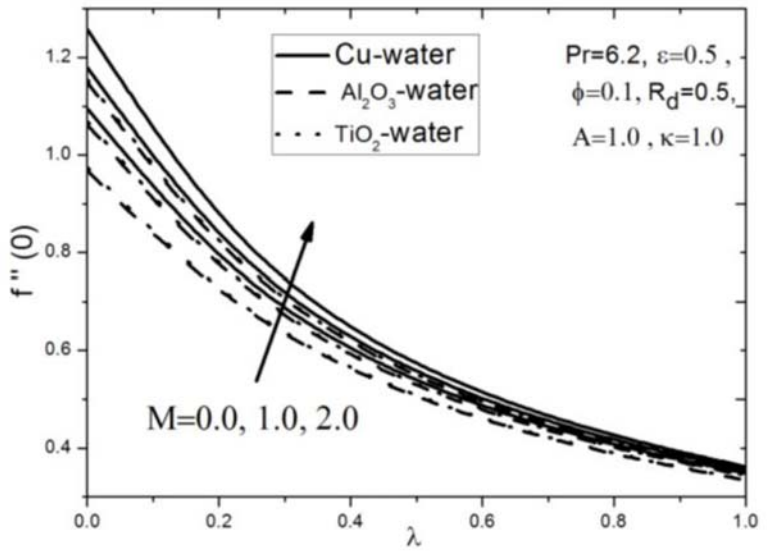

Figure 10. Effects of the magnetic field parameter *M* and λ on the skin friction coefficient.

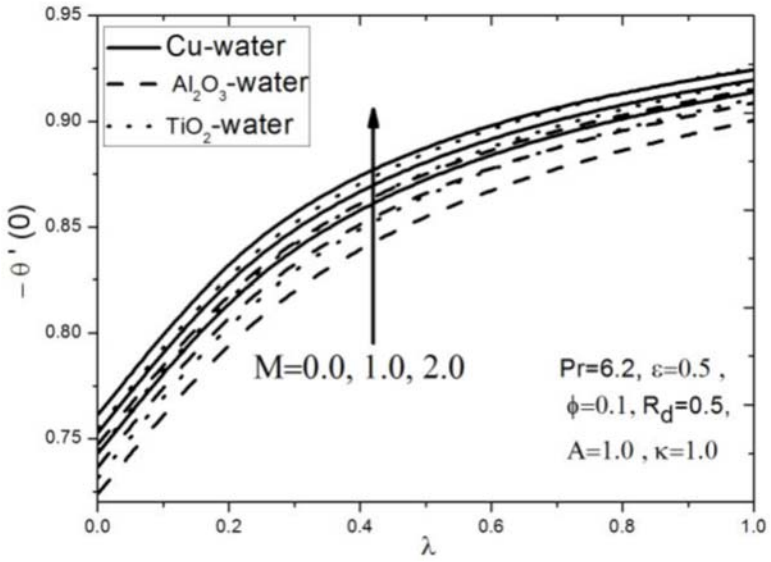

Figure 11. Effects of the magnetic field parameter M and λ on the reduced Nusselt number.

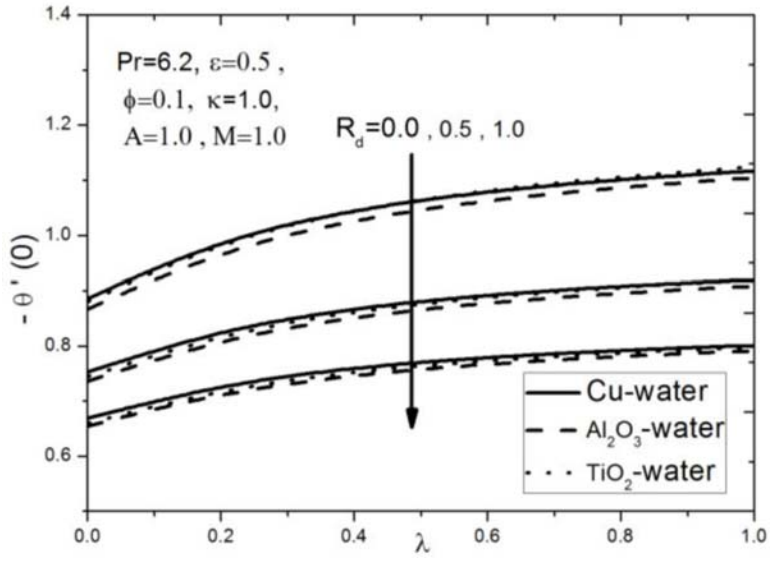

Figure 12. Effects of the radiation parameter R_d and λ on the reduced Nusselt number.

Finally, Figures 13 and 14 depict the variations of skin-friction coefficient $f''(0)$ and Nusselt number $-\theta'(0)$ with stretching parameter ε and slip parameter λ for different nanoparticles. Clearly, ε and λ have the same effects on *Cfr* and *Nur* : an increase in ε and λ reduction of *Cfr* and intensification of *Nur*. Since the fluid flow on the stretching sheet originates from the fluid far from the sheet, velocity of the fluid at the sheet increases with any increase in the slip and stretching parameters; hence, it smoothes interaction between the fluid flow and the sheet, which reduces the skin friction coefficient *Cfr*. This is the reason that the velocity gradient at the surface drops at higher values of ε and λ. What is more, higher velocity at the sheet enhances the momentum near the surface which intensifies the heat transfer rate *Nur* at the surface. It is interesting to see that Cu-water exhibits higher skin-friction coefficient and heat transfer rate compared to Al_2O_3-water and TiO_2-water nanoparticles.

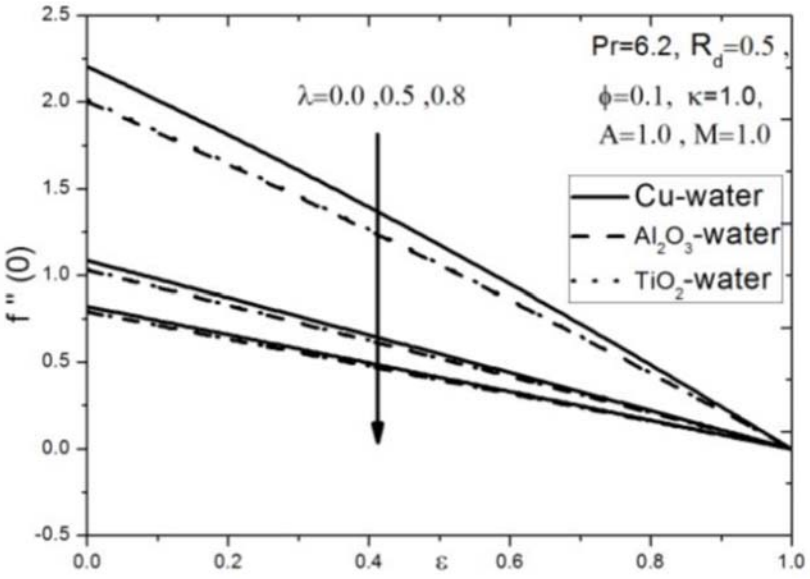

Figure 13. Effects of the slip parameter λ and ε on the skin friction coefficient.

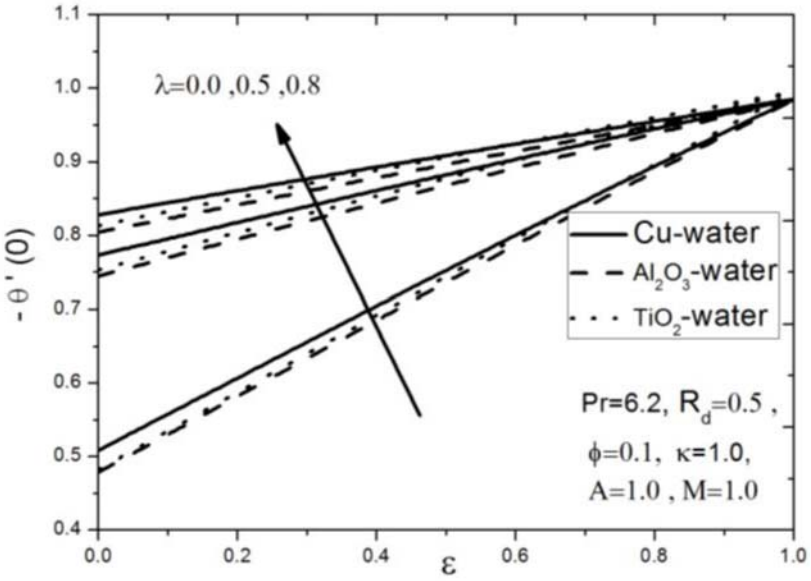

Figure 14. Effects of the slip parameter λ and ε on the reduced Nusselt number.

4. Conclusion

We studied the similarity solutions of the slip flow and heat transfer in unsteady MHD stagnation point flow and heat transfer of a nanofluid adjacent to a linearly stretching sheet in a porous medium in the presence of an applied magnetic field and thermal radiation. The obtained similarity ordinary differential equations are solved by using the fourth-order Runge-Kutta method with shooting technique. The results of the present paper show that the flow velocity and the temperature field are strongly influenced by the slip parameter. The obtained results are displayed graphically to illustrate the influence of the different physical parameters on the fluid flow and heat transfer characteristics as well as the local surface shear stresses and the local Nusselt number. From the present study, the following conclusion are drawn:

(i) Nanofluid velocity profile increases with increase in nanoparticle volume fraction ϕ, the porous media parameter κ, the magnetic field parameter M, the slip parameter λ and the unsteadiness parameter A for Cu-water.

(ii) Temperature profiles increases with increase in the radiation parameter R_d, nanoparticle volume fraction ϕ and the unsteadiness parameter A for Cu-water.

(iii) Skin-friction coefficient increases with increase of porous parameter κ and the magnetic field parameter M, whereas it decreases with increase of the slip parameter λ for different nanoparticles.

(iv) Local Nusselt number decreases with increase in the radiation parameter R_d, whereas it increases with increase of the slip parameter λ, porous parameter κ and the magnetic field parameter M for different nanoparticles.

(v) Cu-water is found to have higher skin-friction coefficient and heat transfer rate when compared with Al_2O_3-water and TiO_2-water nanofluids.

The study of nanofluids is still at its early stage, so that complementary works are necessary to understand the flow and heat transfer characteristics of nanofluids.

References

[1] C. L. M. H. Navier, Mem. Acad. Sci. Inst. France 1 (1823), 414-416.

[2] S. Goldstein, Modern Developments in Fluid Dynamics, Dover, New York, 2 (1965), 676.

[3] S. Yu and T. A. Ameel, Slip-flow heat transfer in rectangular microchannels, Int. J. Heat Mass Transfer 44 (2002), 4225-4234.

[4] C. Derek, D. C. Tretheway and C. D. Meinhart, Apparent fluid slip at hydrophobic microchannel walls, Phys. Fluids 14 (2002), L9-L12.

[5] F. Soltani and U. Yilmazer, Slip velocity and slip layer thickness in flow of concentrated suspensions, J. Appl. Polym. Sci. 70 (1998), 515-522.

[6] K. Watanebe and H. Mizunuma Yanuar, Slip of Newtonian fluids at solid boundary, JSME Int. J. Ser. B 41 (1998), 525.

[7] K. Watanebe and H. Udagawa Yanuar, Drag reduction of Newtonian fluid in a circular pipe with a highly water-repellant wall, J. Fluid Mech. 381 (1999), 225.

[8] E. Ruckenstein and P. Rahora, On the no-slip boundary conditions of hydrodynamics, J. Colloid Interface Sci. 96 (1983), 448.

[9] W. Jr. Marques, G. M. Kremer and F. M. Shapiro, Coutte flow with slip and jump boundary conditions, Continumm Mech. Thermodynam. 12 (2000), 379-386.

[10] A. R. A. Khaled and K. Vafai, The effect of the slip condition on stokes and coutte flows due to an oscillating wall: Exact solutions, Int. J. Nonlinear Mech. 39 (2004), 795-809.

[11] O. D. Makinde and E. Osalusi, MHD steady flow in a channel with slip at the permeable boundaries, Rom. J. Phys. 51(3-4) (2006), 319-328.

[12] C. Y. Wang, Liquid film on an unsteady stretching sheet, Q. Appl. Math. 48 (1990), 601.

[13] N. Bachok, A. Ishak and I. Pop, The boundary layers of an unsteady stagnation-point flow in a nanofluid, International Journal of Heat and Mass Transfer 55(23-24) (2012), 6499-6505.

[14] M. Suali, N. M. A. Nik Long and N. M. Ariffin, Unsteady stagnation point flow and heat transfer over a stretching/shrinking sheet with suction or injection, J. Appl. Math. doi:10.1155/2012/781845, 2012.

[15] T. G. Fang, J. Zhang and Y. F. Zhong, Unsteady viscous flow over an expanding stretching cylinder, Chin. Phys. Lett. 28 (2011), 124707.

[16] A. Malvandi, F. Hedayati and D. D. Ganji, Slip effects on unsteady stagnation point flow of a nanofluid over a stretching sheet, Powder Technology 253 (2014), 377-384.

[17] C. D. S. Devi, H. S. Takhar and G. Nath, Unsteady mixed convection flow in stagnation region adjacent to a vertical surface, Heat Mass Transfer 26 (1991), 71-79.

[18] E. M. A. Elbashbeshy and M. A. A. Bazid, Heat transfer over an unsteady stretching surface, Heat Mass Transfer 41 (2004), 1-4.

[19] R. Tsai, K. H. Huang and J. S. Huang, Flow and heat transfer over an unsteady stretching surface with non-uniform heat source, Int. Commun. Heat Mass Transfer 35 (2008), 1340-1343.

[20] A. Ishak, Unsteady MHD flow and heat transfer over a stretching plate, J. Applied Sci. 10(18) (2010), 2127-2131.

[21] S. R. Pop, T. Grosan and I. Pop, Radiation effect on the flow near the stagnation point of a stretching sheet, Technische Mechanik 25 (2004), 100-106.

[22] E. Abu-Nada, Application of nanofluids for heat transfer enhancement of separated flows encountered in a backward facing step, Int. J. Heat Fluid Flow 29 (2008), 242-249.

[23] H. Kumar, Radiative heat transfer with hydro magnetic flow and viscous dissipation over a stretching surface in the presence of variable heat flux, Thermal Science 13(2) (2009), 163-169.

[24] N. S. Akbar, S. Nadeem, R. Ul Haq and Z. H. Khan, Radiation effects on MHD stagnation point flow of nanofluid towards a stretching surface with convective boundary condition, Chin. J. Aeronaut. 26(6) (2013), 1389-1397.

[25] S. Nadeem, R. Ul Haq and Z. H. Khan, Heat transfer analysis of water-based nanofluid over an exponentially stretching sheet, Alexandria Eng. J. 53 (2014), 219-224.

[26] N. Bachok, A. Ishak and I. Pop, On the stagnation-point flow towards a stretching sheet with homogeneous-heterogeneous reactions effects, Commun. Nonlinear Sci. Numer. Simul. 16 (2011), 4296-4302.

[27] H. F. Oztop and E. Abu-Nada, Numerical study of natural convection in partially heated rectangular enclosures filled with nanofluids, Int. J. Heat Fluid Flow 29 (2008), 1326-1336.

[28] A. Raptis, Radiation and free convection flow through a porous medium, Int. Commun. Heat Mass Transf. 25 (1998), 289-295.

[29] M. Q. Brewster, Thermal Radiative Transfer Properties, John Wiley and Sons, New York, 1972.

[30] E. M. Sparrow and R. D. Cess, Radiation Heat Transfer, Hemisphere, Washington, 1978.

■